Journal of Alloys and Compounds 525 (2012) 159–165

Contents lists available at SciVerse ScienceDirect

Journal of Alloys and Compounds

journal homepage: www.elsevier.com/locate/jallcom

The effect of Zn on the microarc oxidation coating behavior of synthetic Al–Zn binary alloys

Yucel Gencer*, Ali Emre Gulec

Gebze Institute of Technology, Department of Materials Science and Engineering, 41400 Gebze, Kocaeli, Turkey

ARTICLE INFO

Article history:
Received 21 December 2011
Received in revised form 9 February 2012
Accepted 13 February 2012
Available online xxx

Keywords:
Microarc oxidation (MAO)
Plasma electrolytic oxidation (PEO)
Ceramic coating
Al–Zn alloys
Alumina

ABSTRACT

The synthetic Al–Zn binary alloys were prepared in a vacuum/atmosphere-controlled furnace with the addition of 1, 4, 8, 10, 15 and 33 wt.% Zn. The alloys and pure Al were coated by microarc oxidation in the electrolyte containing sodium silicate and potassium hydroxide for 120 min. XRD, scanning electron microscope (SEM)–energy-dispersive X-ray spectroscopy (EDS), profilometry and Vickers microhardness measurements were employed for the characterization of the coating. The higher amount of Zn in the substrate promoted the formation of porous coating. The outer regions of all coatings were loose and weak, while the inner regions were relatively denser and harder. The features on the coating surface became coarser with the increase of Zn content in the alloys, which resulted in the increase of surface roughness from 9.3 μm to 12.5 μm. The coating thickness increased from 80 μm to 120 μm with the increase of Zn content in the substrates. Mullite and γ-Al_2O_3 phases were formed on all coatings and α-Al_2O_3 phase was also formed on coated pure Al and Al–Zn alloys with 1–10 wt.% Zn. Increasing amount of Zn in the Al–Zn alloys suppressed α-Al_2O_3 formation and reduced the microhardness of the coatings. The Zn concentration was constant throughout the coating for the alloys with lower amount of Zn, though it decreased gradually from interface to surface for the alloys containing higher amount of Zn.

1. Introduction

Aluminum alloys containing Zn as one of major alloying elements (7000 series) are mostly preferred in aerospace, automotive and textile industries for their attractive mechanical properties such as high strength/weight ratio, high toughness and very high ductility. Addition of Zn into these alloys improves castability, mechanical properties and helps to overcome hot tearing [1–4]. However, the addition of Zn element deteriorates the atmospheric corrosion resistance of the 7000 series Al alloys and so this limits the usage of these alloys [5].

Therefore a suitable coating is needed to improve the corrosion resistance of the 7000 alloys. Anodizing is an important surface modification technique applied extensively to Al based alloys to improve their surface properties. However, this method is harmful to the environment due to the acidic electrolytes. Furthermore, coatings obtained using anodizing are relatively thinner and have low hardness, thus it does not meet the needed requirements [6–8]. For that reason, a novel method called microarc oxidation (MAO) also known as plasma electrolytic oxidation (PEO) is applied to acquire hard oxide coatings on aluminum and its alloys because of its unique properties such as excellent adhesion to the substrate, high thickness, hardness, corrosion and wear resistance [6,7,9–11].

There are several parameters affecting MAO coating properties such as, composition of the substrate and electrolyte, process time and temperature, applied voltage and current density [7,9–12]. The studies on the MAO coating process and characterization of Al and its alloys concentrated mostly on the effects of electrical parameters, electrolyte chemical composition and process time on the coating properties [7,11–13]. The effect of chemical composition of the substrate, which is also an important process parameter, was studied indirectly in some limited research by choosing different commercial aluminum alloys as substrates with different chemical compositions. Due to the fact that the commercial alloys contain other alloying elements, it is not easy to reveal the individual effect of a certain alloying element. For example, the MAO behavior of 2214-T6 and 7050 Al alloys was studied [14,15]. The substrate materials consisted of different amounts of Zn, Mg and Cu. It was reported that, the growth of α-Al_2O_3 was inhibited on 7050 compared to 2214-T6 and this was attributed to the amount of Zn in the alloys. However, it is not easy to conclude this, because not only Zn amount but also Mg and Cu amounts change in both alloys [15].

The effect of Si, Mg, Cu, Li, Fe in commercial alloys was investigated in another study and it was found that high Si content had an adverse effect on wear resistance of MAO coating [10,14,16,17]. However, it was also reported that Si had a negative and Li had a

* Corresponding author. Tel.: +90 262 605 26 64; fax: +90 262 653 84 90.
E-mail address: gencer@gyte.edu.tr (Y. Gencer).

0925-8388/$ – see front matter © 2012 Elsevier B.V. All rights reserved.
doi:10.1016/j.jallcom.2012.02.094

positive effect on MAO coating formation kinetics. As one of the other alloying element used in Al alloys, Mg has no effect on the coating thickness, yet it slightly decreases the surface roughness [17]. Individual effect of alloying element additions on MAO coating of commercial Al alloys with different content was not clear due to the effect of other alloying elements existing in the alloys [10,18–20]. To our knowledge, only the specific effect of Mg as an alloying element on MAO coating properties on Al alloys was studied in a limited composition range. It was reported that α-Al_2O_3 formation was inhibited when the amount of Mg is higher than 3 wt.% [14]. A recent comprehensive study on the influence of Mg on MAO behavior of aluminum showed that α-Al_2O_3 formation was inhibited and mullite formation was reduced while the coating thickness increased with increasing amount of Mg in the substrate [21].

Zinc is the major alloying element for Al 7000 series alloys, therefore it is important to investigate its specific effect on MAO coating of Al–Zn binary alloys. Although there are several studies on 7000 series Al alloys, the effect of Zn on MAO coating properties is not clear [14,15,22–24]. In this study it is aimed to reveal the specific effect of Zn on MAO coating properties of Al–Zn binary alloys.

For the purpose, synthetic Al–Zn binary alloys were prepared under a vacuum/atmosphere controlled furnace with addition of 1, 4, 8, 10, 15 and 33 wt.% pure Zn into pure aluminum and the substrates characterized. Then, the surfaces of the Al–Zn alloys together with pure aluminum were coated for 120 min under the same electrolyte bath and electrical conditions using MAO system. The coatings were characterized by XRD, scanning electron microscope (SEM)–energy-dispersive X-ray spectroscopy (EDS), and profilometry and microhardness measurements.

2. Experimental

Pure aluminum (99.9%) and pure zinc (99.99%), obtained from Alfa Easer, were used to prepare synthetic Al–Zn binary alloys with 1, 4, 8, 10, 15 and 33 wt.% Zn and these alloys assigned as Al–1Zn, Al–4Zn, Al–8Zn, Al–10Zn, Al–15Zn and Al–33Zn, respectively. The Al–Zn alloys ingots with the dimensions of 80 mm × 50 mm × 25 mm were prepared by melting and casting in a vacuum/argon gas atmosphere controlled furnace. The ingots were sliced to obtain 50 mm × 25 mm × 5 mm Al–Zn alloy substrates for MAO coating. The surface of the specimens were ground using 80–1200 grit emery papers and polished using 3–1 μm diamond paste. After grinding and polishing, the substrate samples were cleaned in an ultrasonic bath of ethanol for 5 min. Pure aluminum samples with the same dimensions were also prepared similarly for comparison purpose. Veeco Dektak 8 profilometer was used to determine the surface roughness of the uncoated Al–Zn substrates. The area of 5 mm × 5 mm was scanned (20 scans) on each sample.

An electrolyte was prepared by dissolving 12 g/l Na_2SiO_3 and 2 g/l KOH in 30 l distilled water. The process was carried out by means of a homemade MAO coating unit with an asymmetric AC power supply. The current density was maintained approximately 0.25 A/cm^2 for each sample. The electrolyte was mixed by pressurized air continuously to keep the electrolyte homogenous and its temperature was kept at 20 °C by circulating cold water around the electrolyte cell during the MAO process. All specimens were MAO coated for the duration of 120 min using the same process parameters. The MAO coated samples were ultrasonically cleaned in deionized water to remove possible electrolyte residues on the coating and dried under flow of warm air.

Bruker D8 advanced X-ray diffractometer with a Cu Kα radiation, over a 2θ range from 10° to 90°, was employed for the phase characterization of coating obtained on Al–Zn binary alloys and pure Al samples. Further XRD scans of the MAO coatings of pure Al, Al–4Zn and Al–33Zn alloys were carried out after removing approximately half the coating thickness by conventional grinding.

The surface roughness of the coated samples was measured by means of the same Profilometer by scanning the same region and parameters used for the bare substrates. The surfaces of coated samples were examined with FEI/Philips XL30 FEG ESEM scanning electron microscope after gold coating. Then the samples were cut into two equal pieces, mounted into epoxy resin, ground and polished to expose the cross-section of the coating. Anton Paar MHT-10 microhardness tester attached to a Zeiss optic microscope was used for Vickers indent formation from substrate to the surface of the coating with the applied loads of 50 g for 10 s. Furthermore, microstructural examination and determination of the chemical composition of the MAO coated samples were carried out by cross-sectional SEM with EDS analysis.

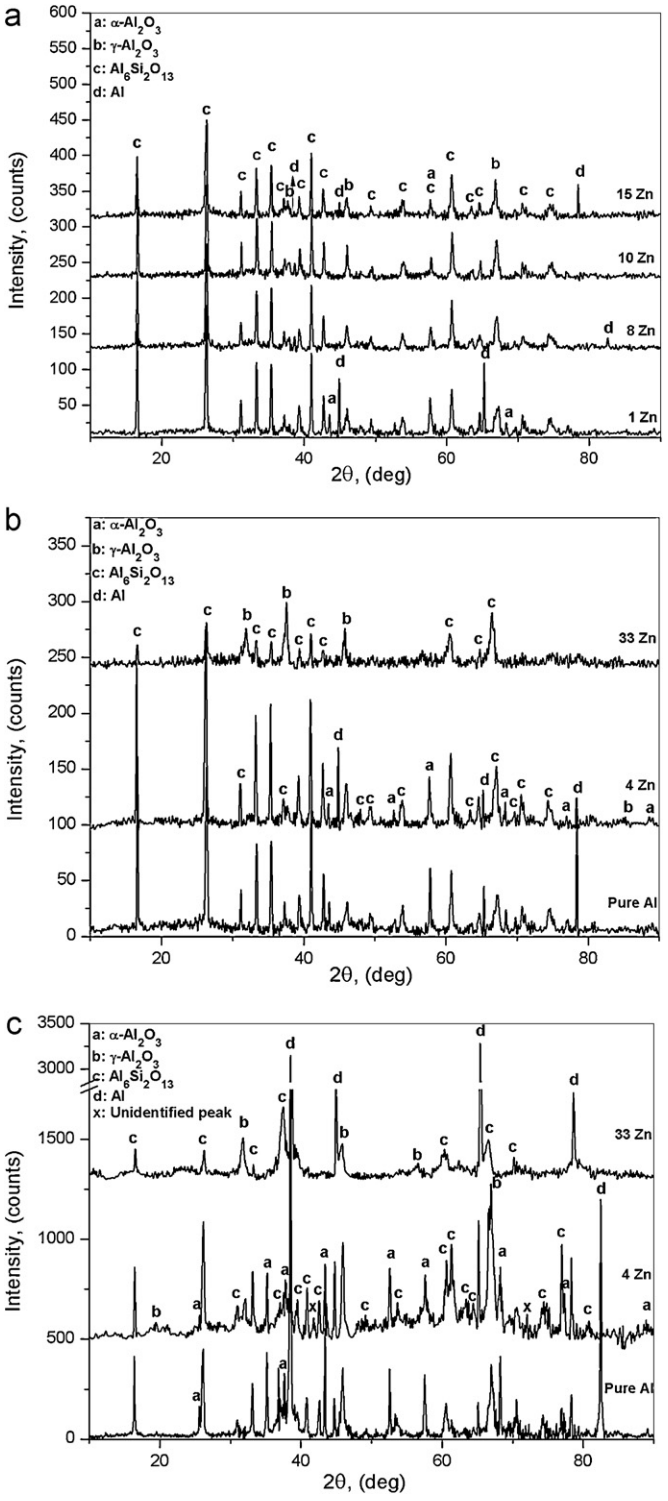

Fig. 1. XRD patterns from surface of MAO coatings: (a) Al–1Zn, Al–8Zn, Al–10Zn, Al–15Zn, (b) pure Al, Al–4Zn, Al–33Zn and (c) surface of ground coatings of pure Al, Al–4Zn, Al–33Zn.

The samples exposing the cross-section of the coating were gold coated before the SEM analysis.

3. Results

The XRD patterns from the surface of MAO coatings of pure Al and Al–Zn (1, 4, 8, 10, 15, 33 wt.% Zn) and from surface of the coating after removing around half the coating thickness were given

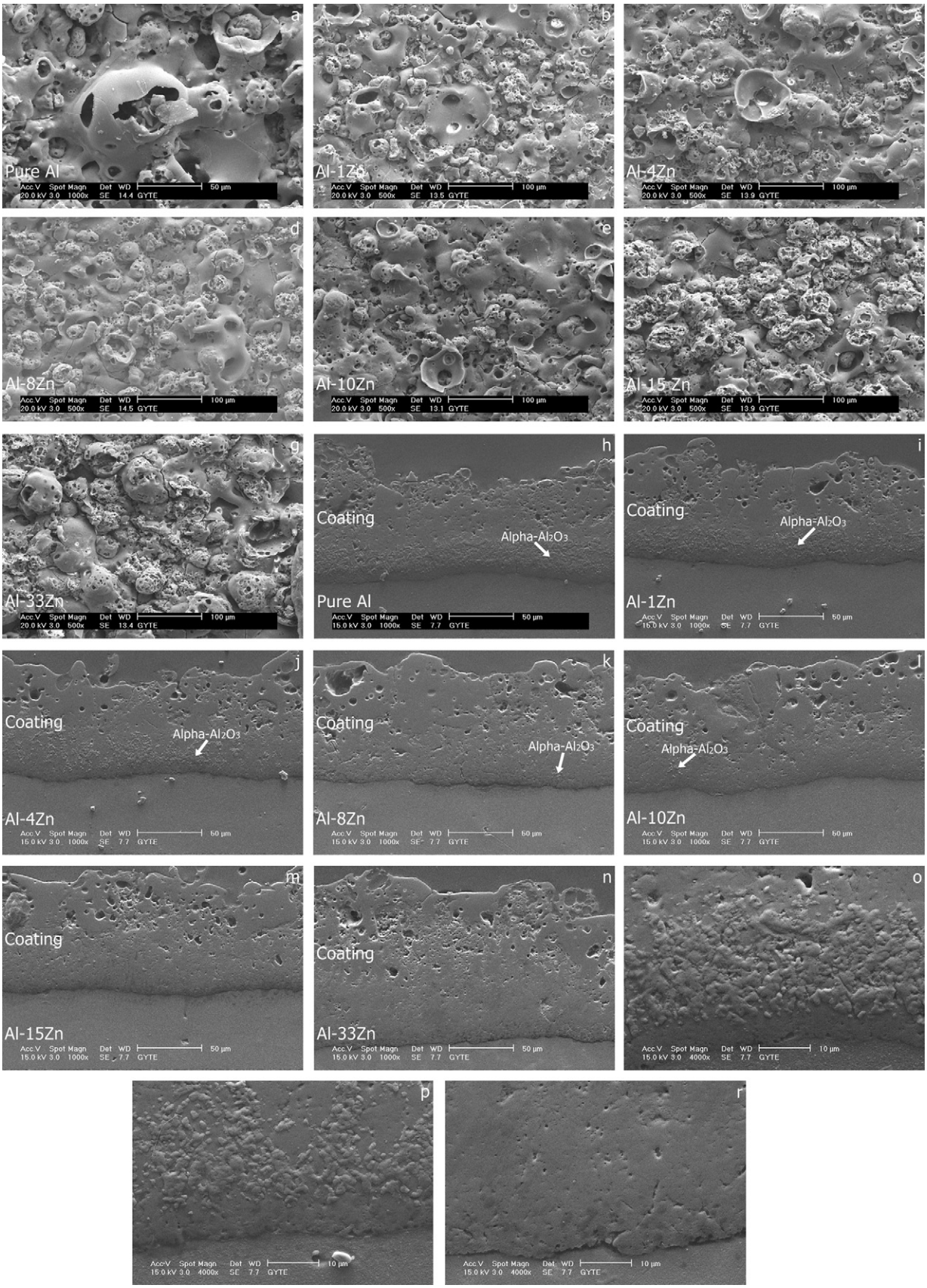

Fig. 2. The surface and cross-sectional SEM micrographs of the MAO coated pure Al and Al–Zn alloys; the surface: (a) pure Al, (b) Al–1Zn, (c) Al–4Zn, (d) Al–8Zn, (e) Al–10Zn, (f) Al–15Zn and (g) Al–33Zn, the cross-sectional: (h) pure Al, (i) Al–1Zn, (j) Al–4Zn, (k) Al–8Zn, (l) Al–10Zn, (m) Al–15Zn, (n) Al–33Zn and higher magnification of the regions close to coating/substrate: (o) Fig 2a, (p) Fig. 2c, (r) Fig. 2n.

in Fig. 1a, b and c, respectively. The surface XRD results show that all coatings consist of mullite ($Al_6Si_2O_{13}$) and γ-Al_2O_3 phases. In addition to these oxide phases the presence of Al originated from the substrate was also evident in XRD pattern for the coatings on Al–Zn alloys up to 15 wt.% Zn containing alloys. The formation of α-Al_2O_3 was also evident for the coatings on Al, Al–1Zn and Al–4Zn on surface XRD patterns (Fig. 1a,b). XRD scans from ground surface of MAO coatings further confirm the presence of α-Al_2O_3 with higher amount in the inner region of the coatings of pure Al and Al–4Zn while the absence of α-Al_2O_3 for the coating of Al–33Zn (Fig. 1c). It should be noted that there are two unidentified peaks with low intensities on XRD pattern of Al–4Zn coating after removing half of the coating layer. Both of the XRD scans from outer surface and inner regions revealed that the intensity of mullite phase decreases with the increasing amount of Zn in the substrate.

The surface SEM images of MAO coated pure Al and Al–Zn alloys are illustrated in Fig. 2a–g. The surface of MAO coated pure aluminum is composed of various sized spherical shaped porous and hollow hemisphere features and the smaller sized spherical features are dominant as shown in Fig. 2a. Some regions of the coating surface have a relatively glassy appearance with some cracks and porosities. A similar appearance with relatively higher amount of glassy regions is evident on the surface of coatings of Al–Zn alloys with 1, 4, 8, 10 wt.% Zn (Fig. 2b–e). The coatings on the Al–15Zn and the Al–33Zn have relatively rougher surfaces with higher amount of sponge-like spherical/hemispherical features. Also similar cracks are noticeable on the surface of all Al–Zn alloys as in the case of the coating on pure Al. Fig. 2h–r illustrates the cross-sectional SEM images of coated pure Al and 1, 4, 8, 10, 15 and 33 wt.% Zn alloys. These images showed that adhesion between substrates and coatings is very well. The interface between the oxide coatings and the substrates are wavy in nature. Outer regions of the coating were loose and porous while inner regions seemed dense. It was seen that the number of these pores was in tendency of increase with increasing Zn content in the substrate material. Precipitates were observed in the regions near coating–substrate interface. The precipitates were seen as bands for the alloys containing Zn up to 4 wt.% (Fig. 2a–j). However, with the increase of Zn element in substrate material, these precipitates tended to disappear. There were relatively very few precipitates in the coating of Al–8Zn and Al–10Zn (Fig. 2k and l). It was not possible to observe these precipitates in the coatings of Al–Zn alloys with Zn content more than 10 wt.% (Fig. 2m and n). The further cross-sectional SEM images taken with higher magnification from the regions near coating–substrate interface of pure Al (Fig. 2h), Al–4Zn (Fig. 2j) and Al–33Zn (Fig. 2n) were given in Fig. 2o, p and r, respectively. The irregular shaped precipitates are more clearly seen for the MAO coatings of pure aluminum (Fig. 2o) and Al–4Zn (Fig. 2p), while the precipitates are much less in the coatings of Al–4Zn and even completely disappeared on the MAO coating of Al–33Zn (Fig. 2r).

The porosities in the outer loose regions are larger than in the inner dense regions for all coatings and are not distributed evenly in the outer loose region of the coatings. The size and number of these round shaped porosities in the coatings increase with amount of zinc in the substrates even in the inner dense region of the coatings. The cross-sectional SEM images show also that, there are microcracks in outer regions of coatings (Fig. 2h–n).

SEM–EDS analysis results of the coating on pure Al and Al–33Zn were illustrated in Fig. 3. Typical SEM–EDS results show that the outer region of the coating is rich in silicon. Although Si was not detected in the dense region of coating and substrate, its relative amount starts to increase from the dense region toward the surface of coating for the coating of pure Al and Al–33Zn (Fig. 3a and b). The presence of the oxygen is almost constant from interface to the surface of the coating (Fig. 3a and b). The relative amount of Al is approximately constant in the substrate, sharply decreases in

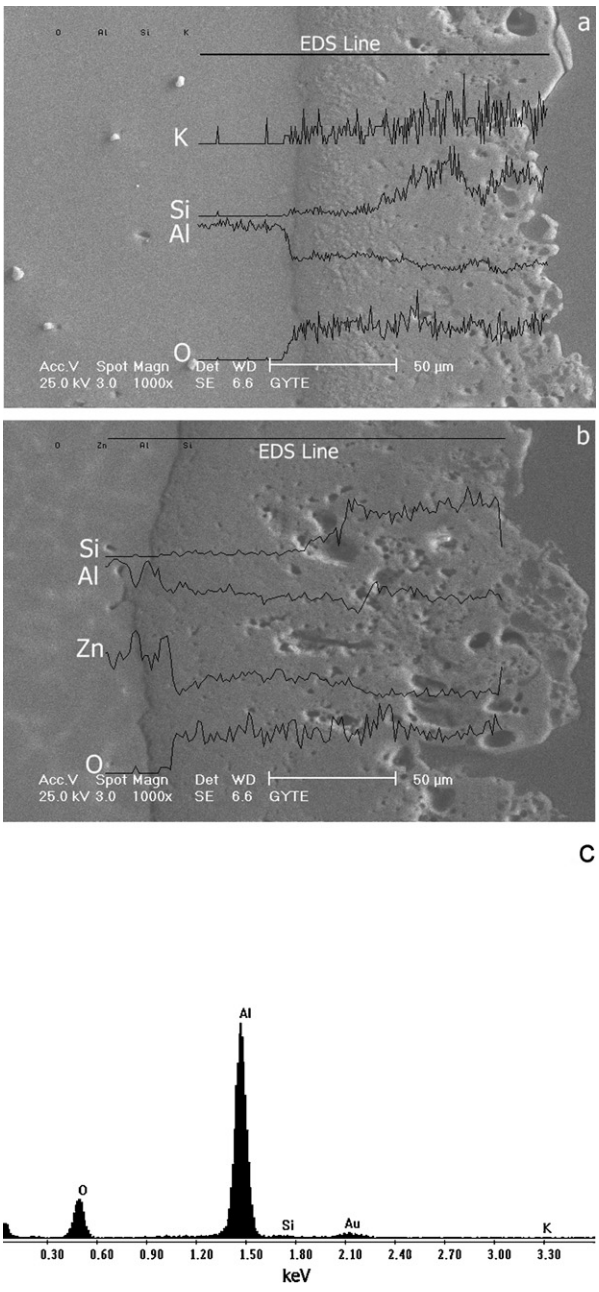

Fig. 3. The cross-sectional micrograph with a typical SEM–EDS analysis results: (a) line SEM–EDS analysis of pure Al, (b) line SEM–EDS analysis of Al–33Zn alloy, (c) spot SEM–EDS analysis of precipitate marked in Fig. 2h.

the substrate/coating interface, more or less invariable in the inner dense region and slightly decreases in the outer loose region of the coating on pure Al (Fig. 3a). K was also detected in the coatings and its relative amount continuously increases from interface to the outer surface of the coating (Fig. 3a). There are some variations in the relative amount of Al and Zn in the substrate. The amount of Zn in the dense region is relatively higher than the amount in loose outer region (Fig. 3b). These SEM–EDS results are typical for the coatings of other Al–Zn alloys. Furthermore, Fig. 3c illustrates the spot SEM–EDS analysis of precipitates marked as "Alpha-Al_2O_3" in Fig. 2h. This spectrum reveals that these precipitates are pure aluminum oxide as they contain only aluminum and oxygen.

Fig. 4 illustrates surface roughness (R_a) of the coated samples change with the amount of Zn in Al–Zn substrates while the surface roughness of the uncoated samples was approximately 0.25 μm.

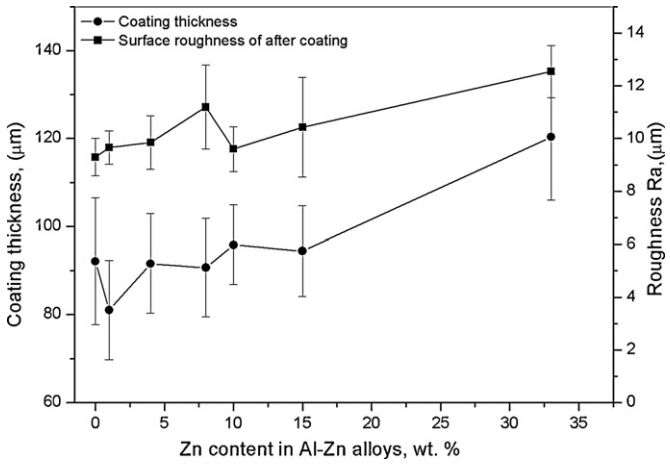

Fig. 4. The change in MAO coating thickness and surface roughness (R_a) with Zn content in Al–Zn alloys.

The average surface roughness value of the coating is 9.3 μm for pure Al and it increases with Zn content in the substrates up to 12.5 μm. Although there is a scattering for the surface roughness values, the increase is approximately linear with Zn content in the substrates.

Fig. 4 also illustrates the average thickness values determined from cross-sectional views of the SEM micrographs. It can be seen that coating thickness values increase with Zn content. The increase is not very significant for the coatings formed on Al–Zn alloys containing 15 wt.% Zn but it increases considerably for the coatings formed on Al–Zn alloys containing 33 wt.% Zn. The lowest thickness value was attained on Al–1Zn and the highest thickness value was attained on Al–33Zn with the average thickness values of 80 μm and 120 μm, respectively. It should be noted that the scattering in the thickness values are really high.

The typical microhardness profiles obtained from the measured microhardness values of Vickers indents for the coatings are illustrated in Fig. 5. The figure reveals that the maximum hardness values were measured at the region close to substrates (10–15 μm to the interface) with a highest value of 1855 HV for the coating of pure Al and the hardness values decrease with distance from substrate–coatings interface for all coatings. The addition of Zn to the substrate results in lower microhardness values obtained from the inner region of the coatings close to coating/substrate interface. The obtained hardness values from the outer region of the coatings were not consistent and consequently they were disregarded due to the presence of many porosities and cracks in those regions.

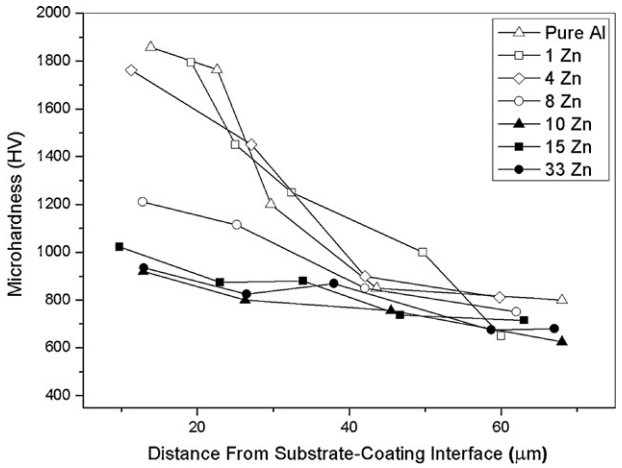

Fig. 5. The microhardness profiles from the substrate/coating interface to the surface of MAO coatings for pure Al and Al–Zn alloys.

4. Discussion

The cross-sectional SEM examination results showed that the Al–Zn alloys coated by MAO consisted of two main regions: (I) Loose, porous, weak outer region and (II) relatively denser, harder inner region.

According to the SEM–EDS analysis, it was thought that the source of the detected Si and K elements in the outer loose region was Na_2SiO_3 and KOH, which were used in electrolyte. The high Si concentration in the outer region promoted the mullite phase formation which was determined by XRD. Since the electrolyte penetrates and accumulates in the plasma channels, a reaction occurred and continued among Al, O and Si due to local high temperature and pressure provided by sparks. The formation of the mullite in the coating was a result of this reaction. As the plasma channels and open pores become larger, accumulation and reaction of the electrolyte in the plasma channels increased and therefore promoted the mullite phase formation in the outer region. In addition to mullite phase formation in the coatings, the formation of γ-Al_2O_3 was detected by XRD analysis. Furthermore, the XRD results (Fig. 1) from the outer surface of coatings and from the surface of ground coatings confirmed the existence of α-Al_2O_3 phase in coatings of pure Al and Al–Zn (1–4 wt.% Zn) alloys. This result is in agreement with the other studies in which the dense region, close to coating/substrate interface of the MAO coatings on aluminum alloys, contains α-Al_2O_3 phase [11,14,18,19,25].

The formation of γ-Al_2O_3 phase in both outer and inner regions was usually reported, but the existence of this phase was more dominant in inner region. The transformation to metastable γ-Al_2O_3 was attributed to the rapid solidification of formed Al_xO_y phase. Since, the surface of the coatings is continuously cooled by the cold electrolyte, γ-Al_2O_3 phase was also observed in outer region along with mullite phase [10].

The inner dense region of the coating has less porosity and band like or individual precipitates formed depending on Zn concentration in the substrates. SEM–EDS results revealed that these precipitates are pure aluminum oxide. As reported in the literature, the precipitates in the dense region close to coating/substrate interface in the form of band or just individual precipitates are α-Al_2O_3 phase [14]. Especially, the increase of intensities of α-Al_2O_3 phase peaks from surface XRD results (Fig. 1b) to ground coatings XRD results (Fig. 1c) further confirms that those precipitates were α-Al_2O_3. This was supported by microhardness measurements in this study as well. The region containing a band of irregularly grown precipitates has higher microhardness values of approximately 1855 HV (Fig. 5) for coated pure Al. Although the microhardness value of fully dense α-Al_2O_3 is comparably higher than this value, lower microhardness values of the coatings may be arisen from microstructural defects existing in the coating such as pores and microcraks.

It should also be noted that although the XRD pattern showed the presence of α-Al_2O_3 phase for the substrates that contain 4 wt.% Zn and less (Fig. 1), its occurrence was also evident for coatings with higher Zn content (Al–8Zn and Al–10Zn) as can be seen in the cross-sectional SEM micrograph (Fig. 2k–l.). The region containing a small amount of α-Al_2O_3 precipitates has lower microhardness values of approximately 920 HV for Al–10Zn (Fig. 5). Absence of α-Al_2O_3 phase peak in the XRD result of Al–8Zn and Al–10Zn is attributable to the high thickness of the coatings and the very low amount of the phase in the coatings.

α-Al_2O_3 phase, in the form of precipitates in the dense region of the MAO coating, is more stable than γ-Al_2O_3 as metastable γ-Al_2O_3 phase can transform to α-Al_2O_3 at temperatures higher than 1273 K [26]. Owing to the low thermal conduction of oxide based ceramic coating, as reported in the previous studies, the thicker MAO coating result in γ-Al_2O_3 phase in the inner regions transform to α-Al_2O_3 due to slow cooling [14,26,27]. In contrast to the findings of the reported studies, the coating thickness increase did not promote the α-Al_2O_3 formation in this study. Since the thickness of the coating increased by the amount of Zn in the Al–Zn alloys (Fig. 4), the α-Al_2O_3 formation was not promoted; even its formation was suppressed (Fig. 1). MAO coated pure Al and low Zn containing Al–Zn alloys (Fig. 2h–j) exhibited α-Al_2O_3 phase yet, its existence diminished with the Zn amount (Fig. 2k–l) and disappeared with higher amount of Zn though the coating thickness increases with Zn amount in the substrates. The complete disappearance of α-Al_2O_3 was also confirmed by XRD results obtained after removal of half of the coating on Al–33Zn (Fig. 1c). This finding is in agreement with the study of commercial Al alloys containing different amount of Zn [15]. It was found that α-Al_2O_3 phase was suppressed with amount of Zn in the alloy. However, the presence of other alloying elements prevented to understand the individual effect of Zn due to their effects on the process [15]. Therefore, it should be noted that it is not easy to claim that the coating thickness and consequently the cooling rate is not the only controlling parameter of transformation from γ-Al_2O_3 to α-Al_2O_3.

Although increasing amount of Zn in substrate material resulted in more Zn penetration to the coating (Fig. 3b), there wasn't any Zn-containing phase even on the coatings of Al–Zn alloys with high Zn content. This was most probably because Zn containing phases were not stable and partially dissolved from coating and transferred to the electrolyte during subsequent microarc formation.

The absence of Zn containing phase might also be attributed to existence of Zn in solid solution in the formed oxide phases. This distributed Zn in the coating resulted in suppression of the formation of α-Al_2O_3 in the coatings. This phenomenon may be attributable to the trace amount of Zn in the alumina matrix of the coating. The higher ionic radius of Zn^{+2} than that of Al^{+3} and different valance value distorted and disturbed the lattice and electronic structure of alumina. Therefore, Zn amount in Al–Zn substrate and consequently the trace amount of Zn in the coating might have suppressed transformation from γ-Al_2O_3 to α-Al_2O_3. In addition to the suppression of α-Al_2O_3 formation, the overall microhardness values of the coatings were declined with the increasing amount of Zn in substrate and consequently in the coatings.

The thickness gain may be attributed to porosity formation due to very high evaporation rates of Zn in the coating with high content of Zn in the substrate for the same amount of oxidized material. Furthermore, Zn content also decreased the melting temperature of Al–O mixture. This contributed to the formation of glassy Al–Zn–Si–O mixture, which accumulated on the surface much easier. Therefore, the Zn content in the substrate increased the thickness of coating. The increased amount of Zn content in Al–Zn substrate also raised the coating roughness (Fig. 4) because the micro-sparks intensified with the increasing coating thickness and made surface much more rougher [19]. The coating thickness slightly changed in compositions between pure Al and 15 wt.% Zn. However, there was a remarkable increment in the coating thickness of 33 wt.% Zn containing substrate. It was seen that increasing Zn content in substrate material resulted in rougher coatings. Inner regions of the coatings included finer pores whereas outer regions included coarser ones.

The formation of cracks on the surface of MAO coated samples is attributed to low thermal shock resistance of oxide based ceramic coating by rapid cooling and high pressure created by sequential material transfer through plasma channels. The crack formation was less evident because of the high amount of sponge like features created on the coating of Al–Zn alloys with high content of Zn (Al–15Zn and Al–33Zn).

5. Conclusions

In this study, binary Al–Zn alloys and pure Al were coated by MAO for 120 min. These results were acquired:

1. Well-adhered coatings on the substrates consisted of two main regions: (I) dense inner region, (II) porous and loose outer region. Zn addition increased the porosity level in the coatings.
2. The increase in amount of Zn in Al resulted in a rougher surface.
3. Mullite and γ-Al_2O_3 phases existed on all coatings; α-Al_2O_3 phase was also formed on coated pure Al and Al–Zn alloys with 1–10 wt.% Zn.
4. The α-Al_2O_3 phase was observed mainly in inner region of coating as band of precipitates for low content Zn, these precipitates decrease with increase of Zn and completely disappear with 33 wt.% Zn.
5. Although the coating thickness increased with Zn addition, the formation α-Al_2O_3 was suppressed and consequently hardness value of the coatings decreased.
6. The Zn concentration was constant throughout the coating for the alloys with lower amount of Zn though it decreased gradually from interface to surface for the alloys containing higher amount of Zn.

Acknowledgments

The authors express their thanks to Technicians Adem Sen and Ahmet Nazim for their kind assistance during XRD and SEM experimental studies.

References

[1] M. Alipour, M. Emamy, S.H.S. Ebrahimi, M. Azarbarmas, M. Karamouz, J. Rassizadehghani, Mater. Sci. Eng. A: Struct. 528 (2011) 4482–4490.
[2] A. Deschamps, T. Marlaud, F. Bley, W. Lefebvre, B. Baroux, Acta Mater. 58 (2010) 4814–4826.
[3] K.S. Ghosh, N. Gao, Trans. Nonferr. Met. Soc. China 21 (2011) 1199–1209.
[4] L. Litynska-Dobrzynska, J. Dutkiewicz, W. Maziarz, A. Goral, J. Alloys Compd. 509 (2011) S304–S308.
[5] W.B. Xue, C. Wang, H. Tialn, Y.C. Lai, Surf. Coat. Technol. 201 (2007) 8695–8701.
[6] A. Leyland, X. Nie, H.W. Song, A.L. Yerokhin, S.J. Dowey, A. Matthews, Surf. Coat. Technol. 116 (1999) 1055–1060.
[7] G. Sundararajan, L.R. Krishna, Surf. Coat. Technol. 167 (2003) 269–277.
[8] T. Tsukada, S. Venigalla, J.H. Adair, J. Am. Ceram. Soc. 80 (1997) 3187–3192.
[9] Z.S. Jin, H.H. Wu, B.Y. Long, F.R. Yu, X.Y. Lu, Chin. Phys. Lett. 20 (2003) 1815–1818.
[10] L.R. Krishna, A.S. Purnima, N.P. Wasekar, G. Sundararajan, Metall. Mater. Trans. A 38A (2007) 370–378.
[11] A.L. Yerokhin, X. Nie, A. Leyland, A. Matthews, S.J. Dowey, Surf. Coat. Technol. 122 (1999) 73–93.
[12] A. Polat, M. Makaraci, M. Usta, J. Alloys Compd. 504 (2010) 519–526.
[13] W.B. Xue, Z.W. Deng, Y.C. Lai, R.Y. Chen, J. Am. Ceram. Soc. 81 (1998) 1365–1368.
[14] Y.J. Oh, J.I. Mun, J.H. Kim, Surf. Coat. Technol. 204 (2009) 141–148.
[15] K. Tillous, T. Toll-Duchanoy, E. Bauer-Grosse, L. Hericher, G. Geandier, Surf. Coat. Technol. 203 (2009) 2969–2973.
[16] H. Aydin, A. Bayram, A. Uguz, Abrasive, Mater. Test. 50 (2008) 318–325.
[17] S. Li, Y.H. Liu, S.R. Yu, X.Y. Zhu, B.M. Xu, Trans. Nonferr. Met. Soc. 16 (2006) S1624–S1629.
[18] W.C. Gu, G.H. Lv, H. Chen, G.L. Chen, W.R. Feng, S.Z. Yang, Mater. Sci. Eng. A: Struct. 447 (2007) 158–162.
[19] W.B. Xue, Z.W. Deng, R.Y. Chen, T.H. Zhang, Thin Solid Films 372 (2000) 114–117.
[20] W.B. Xue, C. Wang, Y.L. Li, Z.W. Deng, R.Y. Chen, T.H. Zhang, Mater. Lett. 56 (2002) 737–743.
[21] M. Tarakci, Mater. Charact. 62 (2011) 1214–1221.
[22] N. Godja, N. Kiss, C. Locker, A. Schindel, A. Gavrilovic, J. Wosik, R. Mann, J. Wendrinsky, A. Merstallinger, G.E. Nauer, Tribol. Int. 43 (2010) 1253–1261.

[23] W.H. Liu, A.L. Bao, X.Y. Mao, G.H. Zheng, Key Eng. Mater. 353-358 (2007) 1895–1898.
[24] A. Polat, J. Baxi, Y. Kar, M. Usta, M. Makaraci, H. Liang, H. Ucisik, Tms 2008 Annual Meeting Supplemental Proceedings, vol. 3: General Paper Selections, 2008, pp. 211–216.
[25] J.A. Wharton, R.C. Barik, R.J.K. Wood, K.R. Stokes, R.L. Jones, Surf. Coat. Technol. 199 (2005) 158–167.
[26] S.G. Xin, L.X. Song, R.G. Zhao, X.F. Hu, Surf. Coat. Technol. 199 (2005) 184–188.
[27] L. Yerokhin, L.O. Snizhko, N.L. Gurevina, A. Leyland, A. Pilkington, A. Matthews, J. Phys. D Appl. Phys. 36 (2003) 2110–2120.